A novel method to characterize the angular resolution of soft X-ray grazing incidence telescope*

ZHANG Ya-chao (张亚超)[1,2]**, **LIU Peng** (刘鹏)[1,2], **WANG Xiao-guang** (王晓光)[1], **HE Ling-ping** (何玲平)[1], **and CHEN Bo** (陈波)[1]

1. Changchun Institute of Optics, Fine Mechanics and Physics, Chinese Academy of Sciences, Changchun 130033, China

2. University of Chinese Academy of Sciences, Beijing 100059, China

(Received 27 July 2018; Revised 28 September 2018)

In this paper, a novel method is proposed to characterize the operation-waveband angular resolution of the soft X-ray grazing incidence telescope. According to the method, the first is to restore the "geometric image" by removing the aperture diffraction effect from the resolution testing target image measured at visible waveband. The second is to calculate the operation-waveband resolution testing target image by the convolution of "geometric image", diffraction point spread function and surface scattering point spread function. Finally, the operation-waveband (4.47 nm) angular resolution of 9.72" is calculated according to the operation-waveband resolution testing target image on axis. The method does not need to be performed in vacuum and to place the source away from the solar X-ray grazing incidence telescope, which greatly reduces the testing cost and improves the efficiency for the development of the soft X-ray grazing incidence telescope.

Document code: A **Article ID:** 1673-1905(2019)02-0098-6

DOI https://doi.org/10.1007/s11801-019-8124-3

Solar X-ray grazing incidence telescope (SXT) is one of the most important instruments to explore the mechanisms of the solar activities, such as flare, active region, coronal hole and coronal mass ejection[1-4]. So far, many satellites have been launched with an SXT onboard, such as the GOES-M, GOES-N, GOES-O and GOES-P of the USA which have been launched in 2001, 2006, 2009 and 2010, respectively[5]. The satellites that are scheduled to be launched with an SXT onboard include the solar orbiter of the European space agency (ESA) that is scheduled to be launched in 2018 and the solar-C of Japan that is scheduled to be launched in 2019[2,6].

In order to obtain clear observation images on-orbit, the angular resolution is necessary to be characterized before launching the telescope. The angular resolution of the soft X-ray grazing incidence telescope is usually characterized at the operational waveband, directly[7,8]. In general, the characterizing methods include two kinds. The first is to characterize the angular resolution by illuminating the full pupil of SXT with a wide "collimated" X-ray beam, which requires the X-ray source away from the SXT[7]. A representative X-ray calibration facility for the method is the X-ray Calibration Facility (XRCF) in the Marshall Space Flight Center (MSFC), which has the length of 518 m, stainless steel guide tube between the source and the calibration chamber[9]. The second is to characterize the angular resolution by scanning the full pupil with a narrow "collimated" beam, and the angular resolution is obtained by adding up all the scanning results[8]. A representative X-ray calibration facility for the method is the 30 m X-ray calibration facility of the Institute of Space and Astronautical Science (ISAS) in Japan, which can provide a collimated X-ray beam with a maximum width of 4 mm and a divergence angle of 28"[10]. It is clear to see that these two methods are accurate and reliable enough. However, the giant X-ray calibration facility for the first method is usually quite cost to be built, and the second method is time consuming due to scanning the full pupil with a narrow "collimated" beam. Besides, both of them have to be performed in vacuum since the soft X-ray is easy to be absorbed by the air. Therefore, it is quite difficult to characterize the angular resolution of SXT at operational waveband, conveniently.

In order to reduce the characterizing difficulty, this paper propose a novel method that does not need to be performed in vacuum and does not need to place the source away from the SXT. The method is based on the image quality analysis model of the soft X-ray telescope proposed by James Harvey[11] as shown in Fig.1. The impact factors of the imaging quality for the soft X-ray grazing incidence telescope include geometric aberration, aperture diffraction, surface scattering and miscellaneous residual errors (assignment errors, environmental factors, and machining errors, etc.). Harvey has pointed that the

* This work has been supported by the National Natural Science Foundation of China (No.U1631117).

** E-mail: zyc198902@126.com

convolution of the point spread function (PSF) corresponding to each above factor gives a well approximation to the rigorous PSF of the telescope[11]. That is to say the imaging process of an object by SXT can be regarded as a degradation process of the original image of the object. This means that the original image of the object is degraded by the geometric point spread function (GPSF), aperture diffraction point spread function (ADPSF), surface scattering point spread function (SSPSF) and residual error point spread function (RESPSF).

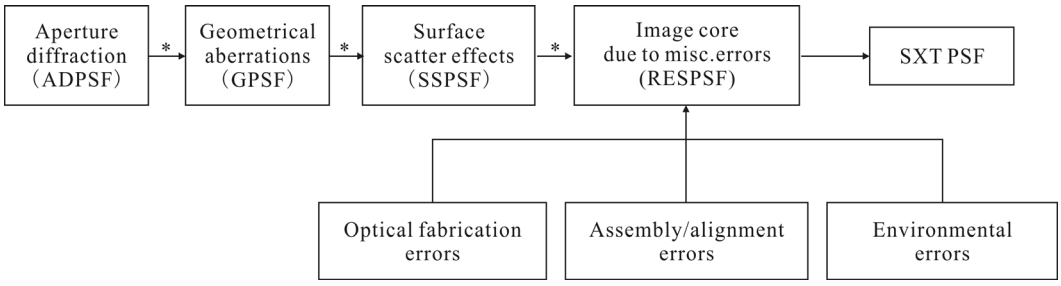

Fig.1 Image quality analysis model of the soft X-ray grazing incidence telescope, where * indicates convolution

The geometric aberration and miscellaneous residual errors are independent of wavelength, while the aperture diffraction and surface scattering are dependent of wavelength. In this paper, the combination of the geometric aberration and miscellaneous residual errors is called as the "focusing error". And the original image degraded by the "focusing error" is called the "geometric image", which can be restored from the measured image at visible waveband by removing the diffraction effect through the image restoration algorithm conveniently. Furthermore, the image formed by the SXT at operational waveband can be calculated by convolution of the "geometric image", operation-waveband ADPSF and SSPSF. Therefore, the operation-waveband resolution testing target image can be obtained from the resolution testing target image at visible waveband, which means that operation-waveband angular resolution can be characterized at visible waveband, indirectly.

The flow chart of the method is shown in Fig.2. First, the "geometric image" $\hat{f}(x,y)$ is obtained by removing the aperture diffraction effect from the resolution testing target image $g(x, y)$ measured at visible waveband by image restoration, since the surface scattering can be negligible at the visible waveband. And then, the operation-waveband resolution testing target image, $g_X(x, y)$, is calculated by convolution of the "geometric image" $\hat{f}(x,y)$, operation-waveband ADPSF and SSPSF. Finally, the angular resolution is calculated from operation-waveband resolution testing target image. According to the above analysis, it is clear to see that the two critical steps of the method are the restoration of "geometric image" and the calculation of operation-waveband SSPSF.

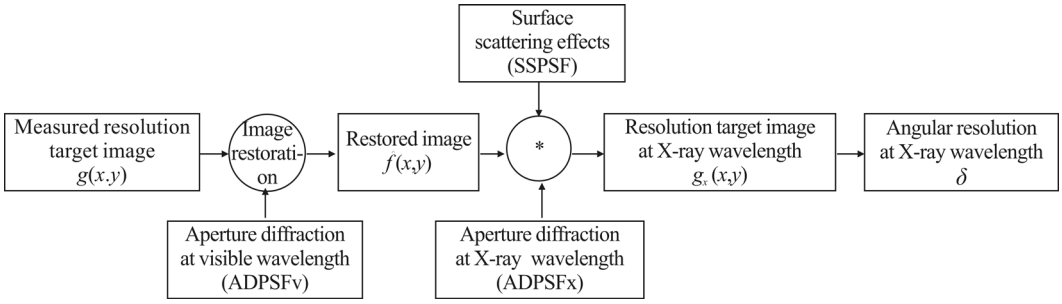

Fig.2 Flow chart of operation-waveband angular resolution testing, where * indicates convolution

The setup of the angular resolution testing system is shown in Fig.3, which is composed of a Newton collimator designed for the angular resolution testing. The focal length of the collimator is 3.75 m, and it has a spherical primary mirror with a diameter of 250 mm, which can produce a parallel beam with a divergent angle less than 2". The source is a tungsten lamp, and a bandpass filter with central wavelength of 570 nm is placed before it to provide a quasi-monochromatic light. The standard USAF1951 resolution testing target is placed on the focal plane of the collimator and illuminated by testing source. Then the collimated beam goes through the SXT and focuses on the CCD placed at focal plane. The pixel size of the CCD is 6.5 μm, and the number of the pixels is 576×720.

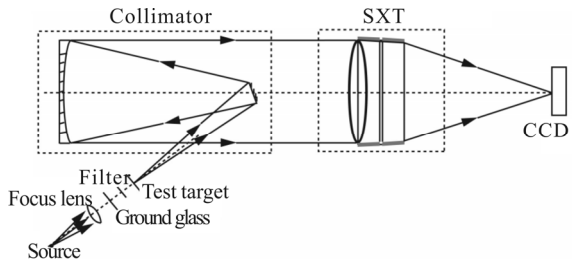

Fig.3 Setup of the angular resolution testing system

The size of the resolution test target is 101.6 mm in length and 81.6 mm in width, and it is made up of 10 groups of resolution bar-sets whose group number are from −2 to 7, and each resolution bar-set group includes 6 pair-lines. The spatial frequency in cycles per millimeter is given by

$$L = 2^{N+\frac{k-1}{6}}, \tag{1}$$

where N and k are the group number and pair number of USAF1951 resolution testing target, respectively. The width of bar-set is then divided by the focal length of the collimator, which results in determination of the angular resolution. In other words, the measured resolution is calculated by

$$\delta_{\mathrm{m}} = \arctan\left(\frac{1}{f_{\mathrm{o}} \cdot L}\right), \tag{2}$$

where f_{o} is the focal length of the collimator.

Fig.4 shows the SXT in our lab, which is Wolter type I designed with the primary and secondary grazing incidence mirrors fabricated in a single naked zerodur substrate. The axial length of each mirror is 47.5 mm with a gap between the two mirrors of 5 mm. The field of view is 42', and the operational waveband ranges from 0.6 nm to 6 nm. The focal length of the SXT is 655 mm. Fig.5 shows the resolution testing target image received by CCD.

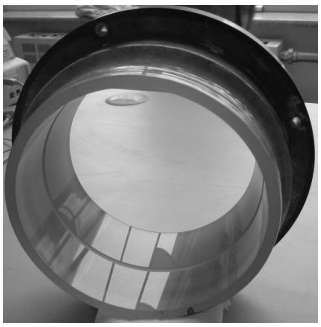

Fig.4 Photo of Wolter type-I soft X-ray grazing incidence mirror in our lab

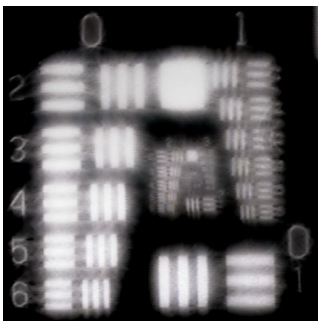

Fig.5 Resolution testing target image at visible waveband (570 nm) received by CCD

The irradiance distribution of aberration-free imaged by an annular aperture with linear obscure ratio of ε is given by

$$PSF_{\mathrm{d}}(r) = \frac{1}{\left(1-\varepsilon^2\right)^2}\left[\frac{2J_1(x)}{x} - \varepsilon^2\frac{2J_1(\varepsilon x)}{\varepsilon x}\right]^2, \tag{3}$$

where $J_1(x)$ is the Bessel function of the first kind, and x is the normalized radius in the focal plane, which is expressed as

$$x = \frac{\pi r}{\lambda f'/D}, \tag{4}$$

where λ is the wavelength, r is the radius in the focal plane, f' is the focal length, and D is the diameter of the optical system, respectively[5]. Fig.6 shows the ADPSF of the telescope at wavelengths of 570 nm and 4.47 nm, respectively.

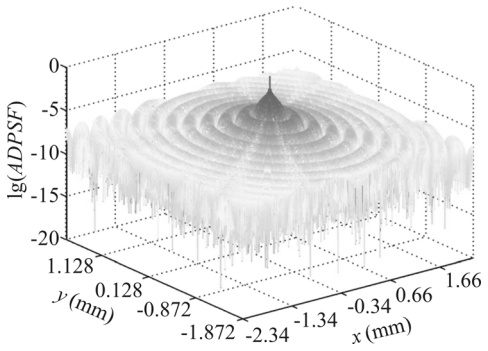

(a) ADPSF at wavelength of 570 nm

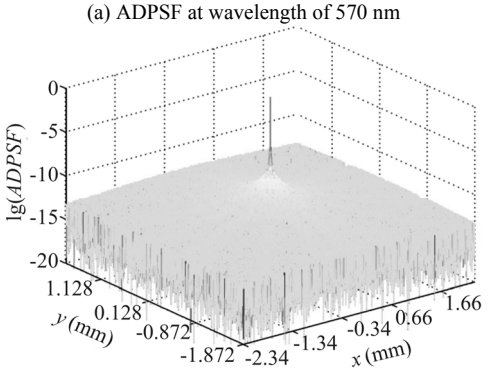

(b) ADPSF at wavelength of 4.47 nm

Fig.6 ADPSF with obscuration ratio ε=0.98

The image restoration methods that are commonly used include Wiener filter, constrained least-square filter and Lucy-Richardson algorithm[12]. Wiener filter and constrained least-squares filter are both linear method, while Lucy-Richardson algorithm is a nonlinear iterative method. As is well known that the image can be affected by various factors during the taking process, and the nonlinear technique is superior than linear technique in many application fields[13]. Therefore, Lucy-Richardson algorithm is adopted for image restoration in this paper. Since the principle and derivation of Lucy-Richardson algorithm is not key for this paper, this only presents the final expression of Lucy-Richardson algorithm and the corresponding iterative formula[12]:

$$f(x,y)=\left\{\frac{g(x,y)}{f(x,y)*h(x,y)}*h(-x,-y)\right\}*f(x,y)\,, \tag{5}$$

$$f_{k+1}(x,y)=\left\{\frac{g(x,y)}{f_k(x,y)*h(x,y)}*h(-x,-y)\right\}*f_k(x,y)\,, \tag{6}$$

where $f(x, y)$ is the original image, $g(x, y)$ is the degraded image, and $h(x, y)$ is the degradation function. Eq.(6) is the iterative formula of Eq.(5), where k is the iterations. The initial value of $f(x, y)$ is $f_0(x, y)$ that is equal to $g(x, y)$. As the iterations increase, $f_k(x, y)$ converges to original image $f(x, y)$ according to probability.

The iterations have to be determined before performing Lucy-Richardson algorithm. In this paper, it is determined by the mean-square error between the measured resolution testing target image $g(x, y)$ and the convolution of the k-loop iterations $f_k(x, y)$, and the ADPSF at visible waveband. When the mean-square error is nearly unchanged, the iteration will be stopped. As shown in Fig.7, the mean-square error is nearly unchanged when the iterations is more than 200. Therefore, the iterations are determined to be 200. And the "geometric image" is shown in Fig.8.

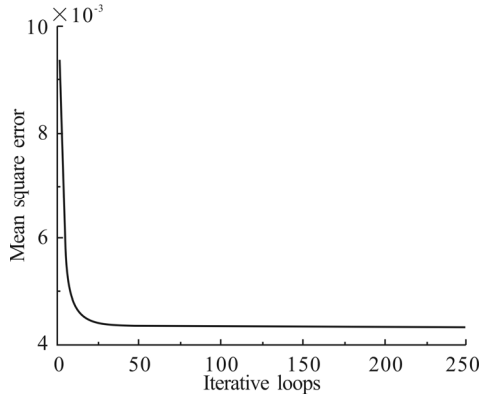

Fig.7 Mean-square error

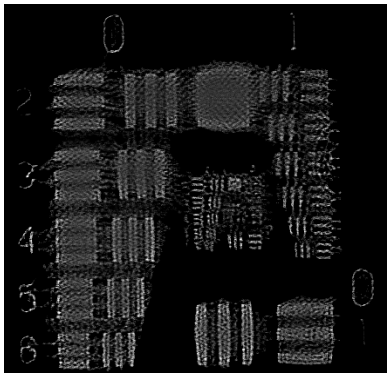

Fig.8 Restored "geometric image" of resolution testing target

The power spectral density (PSD) is required to analyze the surface scattering effect on the angular resolution of the grazing incidence telescope. Since the primary and secondary mirrors are fabricated by the same process, the surface statistics for them are assumed to be identical. Therefore, it only needs to characterize the surface roughness of the primary or secondary mirror. In this paper, we choose to characterize the surface roughness of the secondary mirror.

It often takes different metrological instruments to measure the surface characteristics over the entire range of relevant spatial frequencies. Fig.9 illustrates the metrology data taken from (i) Form Talysurf PGI 1000S, (ii) Zygo surface profiler with a 7.5X objective and (iii) Zygo surface profiler with a 37.5X objective. When the PSDs from different instruments are superposed, an appropriate function can fit to the composite surface PSD. In this paper, the composite surface PSD is fitted with the sum of a Gaussian function, two Lorentzian functions and a K-correlation function, which is expressed as

$$PSD(f)=\sigma_1^2 L_1\sqrt{\pi}\exp\left[-(\pi L_1 f)^2\right]+\frac{2\sigma_2^2 L_2}{1+(2\pi L_2 f)^2}+\frac{2\sigma_3^2 L_3}{1+(2\pi L_3 f)^2}+\frac{A}{\left(1+(Bf)^2\right)^{C/2}}\,, \tag{7}$$

where σ_1, L_1, σ_2, L_2, σ_3, L_3, A, B and C are the fitting parameters. The fitting PSD is shown in Fig.9.

BRDF is calculated according to Harvey-Shack surface scattering theory[15]. Based on the BRDF, the scattering model of the SXT is established in Zemax, and the SSPSF is calculated by non-sequence ray-tracing method[16]. The calculated SSPSF is shown in Fig.10.

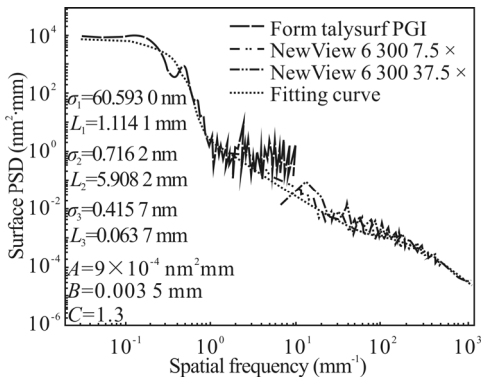

Fig.9 Measured PSDs of the grazing incidence mirror

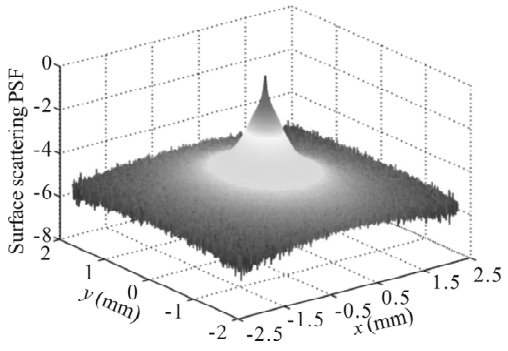

Fig.10 Normalized SSPSF

The operation-waveband resolution testing target image is calculated by the convolution of the ADPSF as shown in Fig.6(b), the "geometric image" as shown in Fig.8 and the normalized SSPSF as shown in Fig.10. The calculated result is shown in Fig.11, where the dotted box region is the key zone. After magnification, the key zone is shown as Fig.12. As shown in Fig.12, the barely resolvable bar-set is 2—4, the line-pair width of which is calculated to be 0.177 mm according to Eq.(1). And then, the operation-waveband (4.47 nm) angular resolution is calculated to be 9.72" on axis according to Eq.(2).

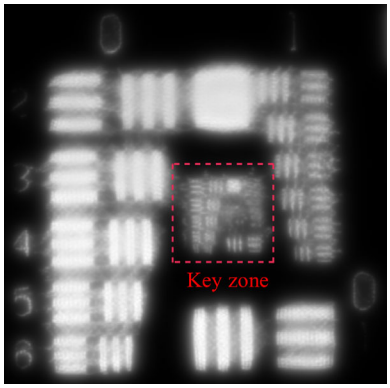

Fig.11 Resolution testing target image at operational waveband (4.47 nm)

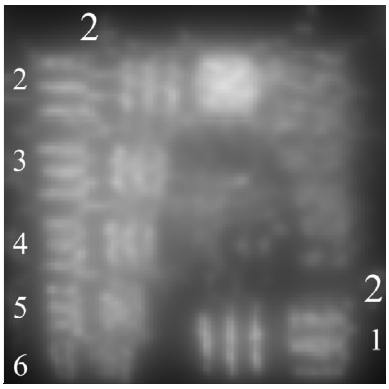

Fig.12 Key zone of Fig.11, where the numbers of the set-bars are noted by the author

The final step is to insure the accuracy of the angular resolution characterized by the novel method. Since the optical parameters of the SXT are nearly identical to those of the solar X-ray imager (SXI) onboard GOES-12 satellite[17], it can be assumed that its angular resolution is quite close to that of the SXI. Fig.13 shows the PSF of the SXI at operational waveband (4.47 nm) on axis[18]. The image of the key zone formed by SXI is shown in Fig.14 which is obtained by convolving the PSF of the SXI with the "key zone" of the resolution testing target. As is shown in Fig.14, the barely resolvable bar-set is 2—4, and the width of the line pair is calculated to be 0.177 mm according to Eq.(1). And then, the angular resolution of the SXI on axis of 9.72" is calculated at operational waveband (4.47 nm) according to Eq.(2). Therefore, the angular resolution of the SXT is close to 9.72" at operational waveband (4.47 nm). This indicates that the angular resolution of the SXT characterized by the novel method is quite close to the angular resolution at operational waveband (4.47 nm), which insures the accuracy of the angular resolution characterized by the novel method.

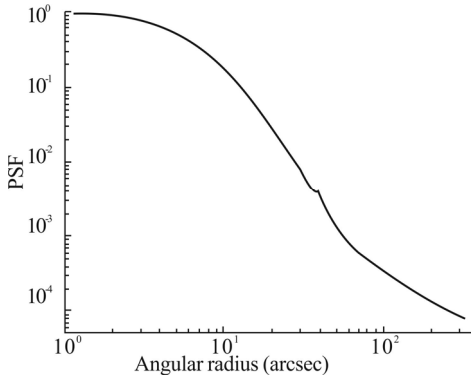

Fig.13 PSF of the SXI onboard GOES-12 at wavelength of 4.47 nm

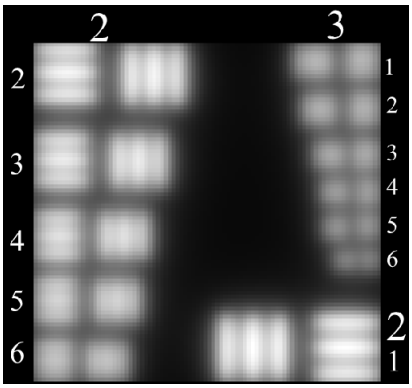

Fig.14 Image of key zone obtained by SXI onboard GOES-12, where the numbers of the set-bars are noted by the author

In summary, a novel method is proposed to characterize the operation-waveband angular resolution of the soft X-ray grazing incidence telescope based on the image quality analysis model of the soft X-ray telescope. The SSPSF is calculated based on Harvey-Shack surface scattering theory. And then it is discussed in detail to restore the "geometric image" from the resolution testing target image measured at visible waveband. Finally, the operation-waveband resolution testing target image is obtained by the convolution of "geometric image", operation-waveband ADPSF and SSPSF, according to which the operation-waveband (4.47 nm) angular resolution of 9.72" is calculated. The method does not need to be performed in vacuum and does not need to place the source away from the SXT, which greatly reduces the testing cost and improves the efficiency for the development of the X-ray grazing incidence telescope.

References

[1] Taro Sakao, Satoshi Matsuyama, Takumi Goto, Jumpei Yamada, Shuhei Yasuda, Kazuto Yamauchi, Yoshiki Kohmura, Ayumi Kime, Akira Miyake, Tadakazu Maezawa, Hirokazu Hashizume, Yoshinori Suematsu, Noriyuki Narukage and Shin-nosuke Ishikawa, SPIE **10386**, 103860E (2017).

[2] Taro Sakao, Noriyuki Narukage, Yoshinori Suematsu, Kyoko Watanabe, Masumi Shimojo, Shinsuke Imada, Shin-nosuke Ishikawa and Edward E. Deluca, SPIE **9144**, 91443D (2014).

[3] James R. Lemen, Dexter Duncan, Christopher Edwards, Frank M. Friedlaender, Bruce Jurcevich, Mons D. Morrison, Larry A. Springer, Robert A. Stern, Jean-Pierre Wulser, Marilyn E. Bruner and Richard C. Catura, SPIE **5171**, 65 (2004).

[4] Hao Yuting, The Design and Realization for high Resolution Solar Soft X-ray CCD Sensor System, University of Chinese Academy of Sciences, Master Dissertation, 10 (2015). (in Chinese)

[5] Li Shun, The Study of Soft X-ray Grazing Incidence Imaging Optical System Design and Testing Technology, University of Chinese Academy of Sciences, PHD Dissertation, 22 (2012). (in Chinese)

[6] S. Krucker, M. Bednarzik, O. Grimm, G. J. Hurford, O. Limousin, A. Meuris, P. Orleanski, K. Seweryn, K. R. Skup, Nuclear Instruments and Methods in Physics Research A **824**, 626 (2016).

[7] Martina Atanassova, Optimizing the Performance of As-Manufactured Grazing Incidence X-Ray Telescopes Using Mosaic Detector Arrays, University of Central Florida, PHD Dissertation, 86 (2005).

[8] Ryo Iizuk, Takayuki Hayashi, Yoshitomo Maeda, Manabu Ishida, Kazuki Tomikawa, Toshiki Sato,aomichi Kikuchi, Takashi Okajima, Yang Soong, Peter J. Serlemitsos, Hideyuki Mori, Takanori Izumiya,and Sari Minami, Journal of Astronomical Telescopes, Instruments, and Systems **4**, 011213-1 (2018).

[9] Edward West, Steve Pavelitz, Ken Kobayashi, Brian Robinson and Jonathan Cirtain, SPIE **8147**, 81471A-1 (2011).

[10] Takayuki Hayashi, Toshiki Sato, Naomichi Kikuchi, Sho Kurashima, Nozomi Nakaniwa, Takuro Sato, Ryo Iizuka, Yoshitomo Maeda and Manabu Ishida, Journal of Astronomical Telescopes, Instruments, and Systems **1**, 044004-1 (2015).

[11] James Harvey, Applied Optics **54**, 2224 (2015).

[12] Hou Yan-peng, Study of Head Motion Blur CT Image Restoration Technology Based on Lucy-Richardson Algorithm, Harbin University of Science and Technology, Master Dissertation, 26 (2016). (in Chinese)

[13] Qiu Xiang, Research on UAV Remote Sensing Blurred Image Restoration Technology,University of Chinese Academy of Sciences, PHD Dissertation, 37 (2017). (in Chinese)

[14] Qiu Li-jie, Application of Lucy-Richardson Algorithm to Astronomical Image and Its Discussion, Jinan University, Master Dissertation, 25 (2011). (in Chinese)

[15] James E. Harvey and Richard N. Pfisterer, SPIE **9961,** 99610E-1(2016).

[16] ZEMAX User's Guide, 420 (2016).

[17] S. M. Hill, V. J. Pizzo, C. C. Balch, D. A. Biesecker, P. Bornmann, E. Hildner, L. D. Lewis, R. N. Grubb, M. P. Husler, K. Prendergast, J. Vickroy, S. Greer, T. Defoor, D. C. Wilkinson, R. Hooker, P. Mulligan, E. Chipman, H. Bysal, J. P. Douglas, R. Reynolds, J. M. Davis, K. S. Wallace, K. Russell, K. Frestone, D. Bagdigian, T. Page, S. Kerns, R. Hoffman, S. A. Cauffman, M. A. Davis, R. Studer, F. E. Berthiaume, T. Saha, G. D. Berthiume, H. Farthing and F. Zimmermann, Solar Physics **226**, 255 (2005).

[18] V. J. Pizzo, S. M. Hill, C. C. Balch, D. A. Biesecker, P. Bornmann, E. Hildner, R. N. Grubb, E. G. Chipman, J. M. Davis, K. S. Wallace, K. Russell, S. A. Cauffman, T. T. Saha and G. D. Berthiume, Solar Physics **226**, 283 (2005).